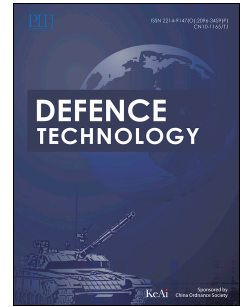


Journal Pre-proof

Observer-based robust high-order fully actuated attitude autopilot design for spinning glide-guided projectiles

Wei Wang, Yuchen Wang, Shiwei Chen, Yongcang Guo, Zhongjiao Shi



PII: S2214-9147(23)00300-8

DOI: <https://doi.org/10.1016/j.dt.2023.11.012>

Reference: DT 1358

To appear in: *Defence Technology*

Received Date: 29 June 2023

Revised Date: 13 October 2023

Accepted Date: 5 November 2023

Please cite this article as: Wang W, Wang Y, Chen S, Guo Y, Shi Z, Observer-based robust high-order fully actuated attitude autopilot design for spinning glide-guided projectiles, *Defence Technology* (2023), doi: <https://doi.org/10.1016/j.dt.2023.11.012>.

This is a PDF file of an article that has undergone enhancements after acceptance, such as the addition of a cover page and metadata, and formatting for readability, but it is not yet the definitive version of record. This version will undergo additional copyediting, typesetting and review before it is published in its final form, but we are providing this version to give early visibility of the article. Please note that, during the production process, errors may be discovered which could affect the content, and all legal disclaimers that apply to the journal pertain.

© 2023 China Ordnance Society. Publishing services by Elsevier B.V. on behalf of KeAi Communications Co. Ltd.

Observer-based robust high-order fully actuated attitude autopilot design for spinning glide-guided projectiles

Wei Wang¹, Yuchen Wang¹, Shiwei Chen¹, Yongcang Guo², Zhongjiao Shi^{1,*}

¹ School of Aerospace Engineering , Beijing Institute of Technology, Beijing 10081, China

² Northwest Industries Group CO., Ltd., Xi'an, 710043, China

* Corresponding author. Email: shizj@ bit.edu.cn

Journal Pre-proof

Observer-based robust high-order fully actuated attitude autopilot design for spinning glide-guided projectiles

Abstract

This paper investigates the design of an attitude autopilot for a dual-channel controlled spinning glide-guided projectile (SGGP), addressing model uncertainties and external disturbances. Based on fixed-time stable theory, a disturbance observer with integral sliding mode and adaptive techniques is proposed to mitigate total disturbance effects, irrespective of initial conditions. By introducing an error integral signal, the dynamics of the SGGP are transformed into two separate second-order fully actuated systems. Subsequently, employing the high-order fully actuated approach and a parametric approach, the nonlinear dynamics of the SGGP are recast into a constant linear closed-loop system, ensuring that the projectile's attitude asymptotically tracks the given goal with the desired eigenstructure. Under the proposed composite control framework, the ultimately uniformly bounded stability of the closed-loop system is rigorously demonstrated via the Lyapunov method. Validation of the effectiveness of the proposed attitude autopilot design is provided through extensive numerical simulations.

Keywords: Spinning glide-guided projectile; Attitude control; Sliding mode disturbance observer; Fixed-time stable theory; High-order fully actuated approach

1. Introduction

A Spinning Glide-Guided Projectile (SGGP) refers to a gun-launched munition that combines the features of a rolling airframe and fin stabilization, further supplemented with economical navigation, guidance, and control systems [1, 2]. One of the critical requirements for an SGGP during its midcourse phase is to maintain a specific attitude for extended-range flight, necessitating swift and precise attitude tracking. Nevertheless, SGGPs face a host of challenges. These include strong uncertainties in their aerodynamic coefficients and exposure to external disturbances. The control system of an SGGP, in particular, grapples with control coupling issues, a consequence of the vehicle's spinning and the inherent delay in the control system's dynamics. The aforementioned factors not only impair the efficiency of the SGGP's attitude control but also challenge its ability to achieve high-accuracy and stable flight. This considerably amplifies the challenge of ensuring precise and stable flight control for the SGGP system.

Numerous refined strategies have been developed specifically targeting control system design for flight vehicle. Prominent among these contain linear quadratic regulator (LQR) control [3], adaptive control [4], and sliding mode control [5]. All the aforementioned research primarily relies on the state-space descriptions. However, the high-order fully actuated system (HOFAS) method proposed recently, which readily integrates with diverse control techniques like backstepping and adaptive control,

demonstrating significant potential for handling nonlinear system [6]. In Ref. [7], the control issue for robotic system was addressed using the PD feedback law, with the feedback gains determined by the introduced direct parametric approach. Ref. [8] presented an attitude controller for spherical liquid-filled spacecraft based on HOFA approach. Ref. [9] given a adaptive fault tolerance control framework with state observer, which can satisfy different fault-tolerance control scenarios without observation condition. Ref. [10] employed a high-order robust command filtered backstepping (HORCFB) controller using the high-order fully actuated (HOFA) system approach. It addresses trajectory tracking in strict-feedback systems with nonlinear uncertainties without simplifying high-order systems. In Ref. [11], the practical prescribed time control of interconnected nonlinear systems is explored using the HOFA system approach. The research introduces a method to define system output's convergence time and accuracy, irrespective of initial conditions. Ref. [12] proposed a modified HOFA theory and applied to the planar quadrotor modeling, which can achieve arbitrarily assignable eigenstructure. In Ref. [13], the prescribed error performance control for second-order fully actuated system is proposed based on prescribed performance function and sliding mode control technique, which guarantees the closed-loop system converges to zero along the prescribed error trajectory. Nevertheless, the HOFA approach necessitates precise knowledge of system dynamics. While it can withstand minor modeling inaccuracies, it isn't designed to handle significant uncertainties, and the behavior of the closed-loop system is affected by the characteristics of uncertainties. The disturbance observer and controller scheme has become an efficient solution to the nonlinear tracking problem of systems with uncertainties, finding applications in areas such as flight control, robotic, and electronic systems.

Among the various observers, the extended state observer (ESO) and the sliding mode disturbance observer (SMDO) are prominent. SMDOs employ a nonlinear feedback law to guide the estimation error towards convergence on a hypersurface within a finite time interval. Levant's observers, a subset of SMDOs, have been applied in fields like UAV attitude control [14], automotive electronic throttle system control [15], and missile guidance law design [16]. In Ref. [17], a super-twisting SMDO was introduced, ensuring finite-time stability of estimation error dynamics. Although the mentioned SMDOs are effective in estimating disturbances, their static gain design can pose challenges. This not only potentially affects the convergence rate and estimation accuracy, but also introduces the burden of parameter tuning.

Building upon adaptive sliding mode control theory, various observers have been proposed. Refs. [18, 19] presented an adaptive sliding mode disturbance observer (ASMDO) that employs an adjustable adaptive law to optimize the adaptive gain, using the estimation error's norm. Ref. [20] suggested a dual-layer ASMDO based on terminal sliding mode, alleviating the need for disturbance boundedness. Yet, the design of this observer is both conservative and intricate. Ref. [21] offered an enhanced ASMDO, where the signum function is replaced by the hyperbolic tangent function, and a modified adaptive law

with a dead zone is applied to adjust the adaptive gain. In Ref. [22], an ASMDO incorporated a σ -modified adaptive law, ensuring both error and adaptive gains remain bounded. However, the mentioned studies primarily assure only the finite-time convergence of the observer system. While the settling time for a finite-time stable system is adjustable, it remains contingent upon the initial state. Consequently, a shift in the initial estimation error results in a corresponding settling time alteration. Moreover, observer design is essentially addressing the stability issue of the error dynamics system.

Fixed-time stable theory offers a solution, ensuring a consistent settling time regardless of initial conditions [23, 24]. Ref. [24] introduced a robust fixed-time consensus protocol where the dynamics stabilize a first-order integrator system within a fixed time via a fractional power method. Nonetheless, this control law faces the singularity challenge and potential input saturation. Multiple nonsingular terminal sliding mode techniques have been developed to combat the singularity issue [25, 26], but they introduce intricate singularity avoidance clauses and suffer from non-strict convergence during the reaching phase. An innovative solution is the integral sliding mode control (ISMC) methodology. By enveloping the desired dynamics within the integral notation, it avoids producing negative exponents, addressing the singularity challenge. Additionally, ISMC establishes the sliding motion from inception, eliminating the reaching phase. Studies [27, 28] depict an ISMC based robust control law for multi-agent systems where the tracking error trajectory aligns with the nominal control and a variable structure term mitigates the effects of matched disturbance.

In this research, a comprehensive fully actuated system-based attitude autopilot approach for a dual-channel controlled SGGP is introduced. This control strategy incorporates a robust adaptive fixed-time integral sliding mode-based disturbance observer (AFxTISMDO) combined with a HOFAS controller. The primary innovations of this research are outlined as follows:

- A dual-channel control attitude model with control coupling was established. Concurrently, a novel AFxTISMDO, which employs the bounded adaptive law and fixed-time integral sliding mode technique, was proposed. In comparison to the adaptive observers in Refs. [18, 19], the proposed SMDO is demonstrated to ensure fixed-time stability irrespective of initial conditions. Moreover, the potential increase problem of the adaptive law is addressed.
- Under the second-order fully actuated scenario, the nonlinear system was transformed into the constant linear closed-loop system. This transformation allows the closed-loop system to track given reference signals accurately. The introduction of integral feedback signal effectively reduces the steady-state error. To our best knowledge, this represents the inaugural study addressing the SGGP attitude control issue within the HOFAS system.
- Based on the Lyapunov stability theory, the proposed composite attitude ensures closed-loop stability through ultimately uniformly bounded stability.

The remaining sections of this paper are structured as follows: Section 2 presents various definitions and useful lemmas. It also establishes the dynamic model of the SGGP. Section 3 introduces the AFxTISMDO and discusses the design of the attitude autopilot based on the AFxTISMDO and the high-order fully actuated approach. Section 4 provides numerous simulations to demonstrate the performance of the proposed attitude autopilot design. Finally, a brief conclusion is presented in section 5.

2. Preliminaries and problem formulation

2.1. Preliminaries

Definition 1 [23]: Considering the following nonlinear system (1), if the upper bound of the settling time is independent of the initial state x_0 , the origin is said to be fixed-time stable.

$$\dot{x}(t) = F(x(t)), x(0) = x_0 \quad (1)$$

where $x \in \mathbf{R}^n$, $F(x(t))$ is continuous, $F(x(t)): D \rightarrow \mathbf{R}^n$, $F(0) = 0$, and D is an open neighborhood containing the origin.

Lemma 1 [23, 29]: For a Lyapunov function $V(x)$, satisfies

$$\dot{V}(x) \leq -a_1 V(x)^{p_1} - b_1 V(x)^{q_1} + \Theta \quad (2)$$

where $a_1 > 0$, $b_1 > 0$, $0 < p_1 < 1$, $q_1 > 1$, and Θ is a small, bounded, positive constant. Then, $V(x)$ is fixed-time stable. Furthermore, the solution of (2) is bounded by

$$\Omega = \left\{ \lim_{t \rightarrow T} x \mid V(x) \leq \min \left\{ \left(\frac{\Theta}{a_1(1-\Xi)} \right)^{\frac{1}{p_1}}, \left(\frac{\Theta}{b_1(1-\Xi)} \right)^{\frac{1}{q_1}} \right\} \right\} \quad (3)$$

where $\Xi \in (0, 1)$ and the upper bound of the settling time can be expressed as follows:

$$T \leq T_{\max} = \frac{1}{a_1 \Xi (1 - q_1)} + \frac{1}{b_1 \Xi (p_1 - 1)} \quad (4)$$

Lemma 2 [30]: Consider the following scalar system:

$$\dot{y} = -2\beta_1 \sqrt{|\arctan(y)|} (1 + y^2) \operatorname{sgn}(y), \quad y(0) = y_0 \quad (5)$$

where $\beta_1 > 0$; system (5) is fixed-time stable, and the upper bound of the settling time satisfies the following inequation

$$T_s \leq \frac{1}{\beta_1} \sqrt{\frac{\pi}{2}} \quad (6)$$

2.2. Attitude coupling model for a spinning glide-guided projectile

The axial-symmetry spinning glide-guided projectile is shown in Fig. 1. The projectile head is equipped with two pairs of movable canards as the control input for the controlled system, and the deflection of the canards generates the control forces and moments. The tail is equipped with rolling stabilization tail fins, and the installation angle of the oblique tail fins generates the rolling stability torque. In Fig. 1, O is the c.g. (center of gravity) of the projectile, and $O-X_N Y_N Z_N$ represents the nonspinning body coordinate frame.

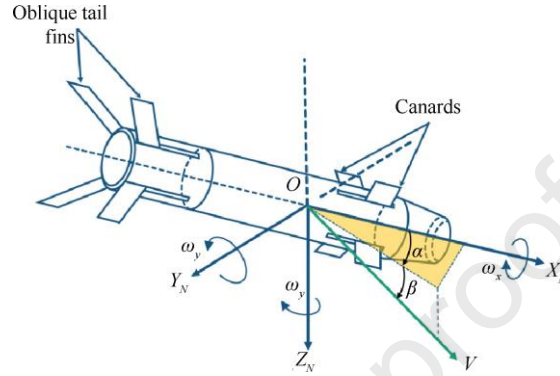


Fig. 1. Diagram of the dual-channel controlled SGGP.

It is assumed that the flight speed and the rolling rate of the projectile body are constant during the midcourse steady flight phase. The attitude model of the dual-channel coupling SGGP can be expressed as follows [31]:

$$\begin{cases} \dot{\alpha} = -\frac{qSc_y^\alpha \alpha - mg \cos \theta}{mV} - \omega_y \tan \theta \cos \alpha \tan \beta + \omega_y \sin \alpha \tan \beta + \omega_z \\ \dot{\beta} = \frac{-qSc_z^\beta \beta + mg \cos \theta}{mV} + \omega_y \tan \theta \sin \alpha + \omega_y \cos \alpha \\ \dot{\omega}_z = \frac{qSL(m_z^\alpha \alpha + m_z^{\omega_z} \omega_z L / V + m_z^{\delta_z} \delta_z)}{J_z} + \frac{J_x \omega_x}{J_z} \omega_y - \frac{J_y \tan \theta}{J_z} \omega_y^2 \\ \dot{\omega}_y = \frac{qSL(m_y^\beta \beta + m_y^{\omega_y} \omega_y L / V + m_y^{\delta_y} \delta_y)}{J_y} - \frac{J_x \omega_x}{J_y} \omega_z + \frac{J_z \tan \theta}{J_y} \omega_y \omega_z \end{cases} \quad (7)$$

where α and β represent the angle of attack and sideslip angle, respectively. ω_z and ω_y are the pitch and yaw angular rates, respectively. θ is the pitch angle, and θ is the flight path angle. m , L , S and V are the mass, reference length, reference area, and flight speed, respectively. q is the dynamic pressure, and g is the gravity acceleration. J_x , J_y and J_z represent the moment of inertia around the projectile body axis. c_y^α and c_y^β are the partial derivatives of the normal force coefficients of the projectile with respect to the angle of attack and the sideslip angle, respectively. m_z^α and m_z^β represent the coefficients of the static stabilization moment. $m_z^{\omega_z}$ and $m_y^{\omega_y}$ are the coefficients of the pitch damping moment. $m_z^{\delta_z}$ and $m_y^{\delta_y}$ are the coefficients of the control moment. δ_z and δ_y are the equivalent canard deflection angles in the pitch and yaw directions, respectively.

2.3. Control coupling model for the canards of a spinning glide-guided projectile

The response lag between the actuator input and output leads to control coupling between the two channels. This so-called control coupling can decrease the flight stability of the closed-loop system. Therefore, it is necessary to establish a dynamic model of canards in the nonspinning projectile body coordinate system. According to related Refs. [32, 33], the dynamics of canards can be expressed by the following second-order system.

$$\frac{\delta(s)}{\delta_c(s)} = \frac{k_s}{T_s^2 s^2 + 2\mu_s T_s s + 1} \quad (8)$$

where δ_c is the canard deflection command and δ is the deflection angle of the canards. k_s , T_s , and μ_s are the gain, time constant and damping ratio of the canards, respectively. In addition, the actual actuator deflections and deflection commands have the following coupling property.

$$\begin{bmatrix} \delta_z \\ \delta_y \end{bmatrix} = k_s k_r \begin{bmatrix} \cos \gamma_d & \sin \gamma_d \\ -\sin \gamma_d & \cos \gamma_d \end{bmatrix} \begin{bmatrix} \delta_{zc} \\ \delta_{yc} \end{bmatrix} \quad (9)$$

where γ_d represents the total delay angle and k_r is the dynamic of the actuator system under spinning. k_r and γ_d are formulated as

$$\begin{cases} k_r = \frac{1}{\sqrt{(1 - T_s^2 \dot{\gamma}^2)^2 + (2\mu_s T_s \dot{\gamma})^2}} \\ \gamma_d = \tau \dot{\gamma} + \arccos \frac{1 - T_s^2 \dot{\gamma}^2}{\sqrt{(1 - T_s^2 \dot{\gamma}^2)^2 + (2\mu_s T_s \dot{\gamma})^2}} \end{cases} \quad (10)$$

2.4. Angle and angular rate loop dynamics of a spinning glide-guided projectile

During actual flight, the influence of gravity is usually counteracted by gravity compensation. In addition, with the control coupling described in Eqs. (9), (7) can be further rearranged as

$$\begin{cases} \dot{\alpha} = -\frac{qSc_y^\alpha \alpha}{mV} - \omega_y \tan \vartheta \cos \alpha \tan \beta + \omega_{y_4} \sin \alpha \tan \beta + \omega_z \\ \dot{\beta} = -\frac{qSc_z^\beta \beta}{mV} + \omega_y \tan \vartheta \sin \alpha + \omega_y \cos \alpha \\ \dot{\omega}_z = \frac{qSL(m_z^\alpha \alpha + m_z^{\bar{\omega}_z} \omega_z L / V)}{J_z} + \frac{J_z \omega_x}{J_z} \omega_y - \frac{J_y \tan \vartheta}{J_z} \omega_y^2 \\ \quad + \frac{qSLm_z^{\delta_z} k_s k_r (\delta_{zc} \cos \gamma_d + \delta_{yc} \sin \gamma_d)}{J_z} \\ \dot{\omega}_y = \frac{qSL(m_y^\beta \beta + m_y^{\bar{\omega}_y} \omega_y L / V)}{J_y} - \frac{J_x \omega_x}{J_y} \omega_z + \frac{J_z \tan \vartheta}{J_y} \omega_y \omega_z \\ \quad + \frac{qSLm_y^{\delta_y} k_s k_r (-\delta_{zc} \sin \gamma_d + \delta_{yc} \cos \gamma_d)}{J_y} \end{cases} \quad (11)$$

where $a_{34} = \frac{qSc_y^\alpha}{mV}$, $b_{34} = \frac{qSc_z^\beta}{mV}$, $a_{24} = \frac{qSLm_z^\alpha}{J_z}$, $b_{24} = \frac{qSLm_y^\beta}{J_y}$, $a_{22} = \frac{qSL^2 \bar{\omega}_z}{2VJ_z}$, $b_{22} = \frac{qSL^2 m_y^{\bar{\omega}_y}}{VJ_y}$,

$$a_{25} = \frac{qSLm_z^{\delta_z} k_s k_r \cos \gamma_d}{J_z}, \quad b_{25} = \frac{qSLm_z^{\delta_z} k_s k_r \sin \gamma_d}{J_y}, \quad a_{26} = \frac{qSLm_z^{\delta_z} k_s k_r \sin \gamma_d}{J_z}, \quad b_{26} = \frac{qSLm_y^{\delta_y} k_s k_r \cos \gamma_d}{J_y},$$

$$c_1 = \frac{J_x \omega_x}{J_z}, \text{ and } c_2 = \frac{J_x \omega_x}{J_y}.$$

Then, system (11) can be described as

$$\begin{aligned} \dot{\boldsymbol{\Omega}} &= \mathbf{F}_a + \mathbf{B}_a \boldsymbol{\omega} + \Delta \mathbf{d}_1 \\ \dot{\boldsymbol{\omega}} &= \mathbf{F}_\omega + \mathbf{B}_\omega \delta_c + \Delta \mathbf{d}_2 \end{aligned} \quad (12)$$

where

$$\begin{aligned} \boldsymbol{\Omega} &= [\alpha, \beta]^T, \boldsymbol{\omega} = [\omega_z, \omega_y]^T \\ \mathbf{F}_a &= \begin{bmatrix} -a_{34}\alpha \\ -b_{34}\beta \end{bmatrix}, \mathbf{B}_a = \begin{bmatrix} 1 & -\tan \vartheta \cos \alpha \tan \beta + \omega_y \sin \alpha \tan \beta \\ 0 & \tan \vartheta \sin \alpha + \cos \alpha \end{bmatrix} \\ \mathbf{F}_\omega &= \begin{bmatrix} a_{24}\alpha + a_{22}\omega_z + c_1\omega_y - \omega_y^2 \tan \vartheta \\ b_{24}\beta + b_{22}\omega_z - c_2\omega_z + \omega_y\omega_z \tan \vartheta \end{bmatrix}, \mathbf{B}_\omega = \begin{bmatrix} a_{25} & a_{26} \\ -b_{25} & b_{26} \end{bmatrix} \\ \Delta \mathbf{d}_1 &= \Delta \mathbf{F}_a + \Delta \mathbf{B}_a \boldsymbol{\omega} + \Delta \mathbf{d}_{1,\text{ext}} \\ \Delta \mathbf{d}_2 &= \Delta \mathbf{F}_\omega + \Delta \mathbf{B}_\omega \delta_c + \Delta \mathbf{d}_{2,\text{ext}} \end{aligned} \quad (13)$$

$\Delta \mathbf{d}_1$ and $\Delta \mathbf{d}_2$ represent the bounded disturbance that contains model uncertainties and external disturbances.

Proposition 1: For the angle loop disturbance,

$$\|\Delta \mathbf{d}_1\| \leq \|\Delta \mathbf{F}_a\| + \|\Delta \mathbf{B}_a\| \|\boldsymbol{\omega}\| + \|\Delta \mathbf{d}_{1,\text{ext}}\| \quad (14)$$

Due to the aerodynamic uncertainties, the external disturbance and the angular rate of the projectile are bounded. Therefore, the disturbance of the angle loop satisfies the following multinomial inequality.

$$\|\Delta \mathbf{d}_1\| \leq \varrho_1 + \varrho_2 \|\boldsymbol{\omega}\| \leq \Delta h_a \quad (15)$$

where ϱ_1, ϱ_2 and Δh_a are three unknown bounded positive constants. Therefore, $\Delta \mathbf{d}_1$ is bounded.

In this paper, following idea of deriving the bounded property for the lumped uncertainty in Refs. [34, 35], if the control signal δ_c , which bounded by

$$\|\delta_c\| < \gamma_1 + \gamma_2 \left\| \int_0^t \boldsymbol{\omega} d\tau \right\| + \gamma_3 \|\boldsymbol{\omega}\| \quad (16)$$

where γ_1, γ_2 , and γ_3 are bounded positive constants, then the lumped uncertainty $\Delta \mathbf{d}_2$ also bounded by

$$\|\Delta \mathbf{d}_2\| < \varsigma_1 + \varsigma_2 \left\| \int_0^t \boldsymbol{\omega} d\tau \right\| + \varsigma_3 \|\boldsymbol{\omega}\| \leq \Delta h_\omega \quad (17)$$

where $\varsigma_1, \varsigma_2, \varsigma_3$ and Δh_ω are four bounded positive constants. The detail proof is given as follows.

Proof: For the total disturbance of the angular rate loop, the multinomial inequation in Eq. (13) is valid.

$$\|\Delta d_2\| = \|\Delta F_\omega\| + \|\Delta B_\omega\| \|\delta_c\| + \|\Delta d_{2,ext}\| \quad (18)$$

Substituting Eq. (16) into Eq. (18) yields

$$\begin{aligned} \|\Delta d_2\| &\leq \Delta F_{\omega} \|\cdot\|_{\max} + \|\Delta B_\omega\| \left(\gamma_1 + \gamma_2 \left\| \int_0^t \omega d\tau \right\| + \gamma_3 \|\omega\| \right) + \|\Delta d_{2,ext}\|_{\max} \\ &= (\Delta F_{\omega} \|\cdot\|_{\max} + \gamma_1 \|\Delta B_\omega\| + \|\Delta d_{2,ext}\|_{\max}) + \gamma_2 \|\Delta B_\omega\| \left\| \int_0^t \omega d\tau \right\| \\ &\quad + \gamma_3 \|\Delta B_\omega\| \|\omega\| \end{aligned} \quad (19)$$

Considering the change in aerodynamic parameters and the boundedness of external disturbances,

$$\begin{aligned} \|\Delta F_\omega\|_{\max} + \gamma_1 \|\Delta B_\omega\| + \|\Delta d_{2,ext}\|_{\max} &< \varsigma_1 \\ \gamma_2 \|\Delta B_\omega\| &< \varsigma_2 \\ \gamma_3 \|\Delta B_\omega\| &< \varsigma_3 \end{aligned} \quad (20)$$

Remark 1: The closed-loop input signal structure in Eq. (16) does not adopt the angular acceleration signal to design the control signal. This is because the measured angular acceleration signal is susceptible to noise pollution. Moreover, if the noise-contaminated signal is used as a component of the control signal, the stability of the closed-loop system in the angular rate loop will be affected.

3. Controller design

In this section, the nonlinear control of Eq. (12) is addressed considering uncertain structures, facilitated by an observer-based HOFAS controller framework. Initially, a novel disturbance observer is introduced. Then, using the estimates from the observer, a controller based on HOFAS and the parametric method is integrated into the system, form a closed loop. The schematic representation of the proposed attitude autopilot is illustrated in Fig. 2.

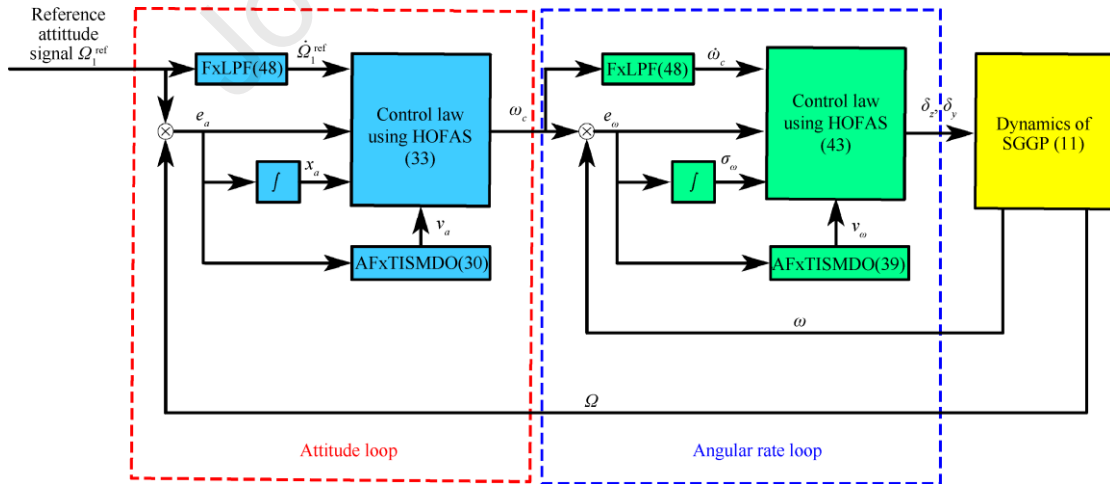


Fig. 2. The control scheme for the dual-channel controlled SGGP attitude autopilot.

3.1. Design of a disturbance observer with fixed-time convergence

The reference angle command is defined as $\Omega_{ref} = [\alpha_{ref}, \beta_{ref}]^T$. The angle tracking error is defined as $e_a = [\alpha - \alpha_{ref}, \beta - \beta_{ref}]^T$. The dynamics of the error can be expressed as follows:

$$\dot{e}_a = \dot{\mathbf{Q}} - \dot{\mathbf{Q}}_{\text{ref}} = \mathbf{F}_a + \mathbf{B}_a \boldsymbol{\omega} + \Delta \mathbf{d}_1 - \dot{\mathbf{Q}}_{\text{ref}} \quad (21)$$

$\boldsymbol{\omega}$ can be regarded as the control input of the angle loop. To extend system (21) to a second-order system, $\mathbf{x}_a = \int_0^t \mathbf{e}_a d\tau$, and its second-order derivative with respect to time is obtained as

$$\ddot{\mathbf{x}}_a = \mathbf{F}_a + \mathbf{B}_a \boldsymbol{\omega} + \Delta \mathbf{d}_1 - \dot{\mathbf{Q}}_{\text{ref}} = \underbrace{(\mathbf{F}_a - \dot{\mathbf{Q}}_{\text{ref}})}_{\bar{\mathbf{F}}_a} + \mathbf{B}_a \boldsymbol{\omega} + \Delta \mathbf{d}_1 \quad (22)$$

where $\bar{\mathbf{F}}_a = \begin{bmatrix} -a_{34}\alpha - \dot{\alpha}_{\text{ref}} \\ -b_{34}\beta - \dot{\beta}_{\text{ref}} \end{bmatrix}$, $\mathbf{B}_a = \begin{bmatrix} 1 & -\cos\alpha \tan\beta \tan\vartheta + \sin\alpha \tan\beta \\ 0 & \sin\alpha \tan\vartheta + \cos\alpha \end{bmatrix}$.

Hence, the attitude tracking problem of the angle loop is transformed into the stability problem of the second order system.

Introduce an auxiliary variable z_a as the estimation value of e_a and the estimation error is defined as $\tilde{z}_a = z_a - e_a$. The first derivative of e_a respect to time is expressed as

$$\dot{\tilde{z}}_a = \dot{z}_a - \bar{\mathbf{F}}_a - \mathbf{B}_a \boldsymbol{\omega} - \Delta \mathbf{d}_1 \quad (23)$$

The desired dynamic of $\dot{\tilde{z}}_a$ is designed as

$$\dot{z}_a = \bar{\mathbf{F}}_a + \mathbf{B}_a \boldsymbol{\omega} - \tilde{z}_{a,\text{nom}} + \mathbf{v}_a \quad (24)$$

where $\tilde{z}_{a,\text{nom}}$ represents the expected dynamic of the estimation error and is designed as follows:

$$\tilde{z}_{a,\text{nom}} = 2\beta_{\text{nom}} \sqrt{\|\arctan(\tilde{z}_a)\|} \left(\mathbf{I}_2 + \tilde{z}_a^2 \right) \text{sgn}(\dot{z}_a) \quad (25)$$

\mathbf{v}_a represents the estimated value of the disturbance. Then, the integral sliding mode vector is defined as

$$\mathbf{s}_a = \tilde{z}_a(t) - \tilde{z}_a(0) + \int_0^t \tilde{z}_{a,\text{nom}} d\tau \quad (26)$$

From the design principle of the integral sliding mode, i.e., $\mathbf{s}_a = \dot{\mathbf{s}}_a = 0$, the following dynamics can be obtained:

$$\dot{\mathbf{s}}_a = \mathbf{v}_a - \Delta \mathbf{d}_1 \quad (27)$$

The virtual control value \mathbf{v}_a can be expressed in the following form.

$$\mathbf{v}_a = -\alpha_a \lceil s_a \rceil^{n_a} - \beta_a \lceil s_a \rceil^{q_a} - \mathbf{K}_h(t) \text{sgn}(s_a) \quad (28)$$

where the symbol $\lceil x \rceil$ refer to $\lceil x \rceil^y = |x|^y \text{sign}(x)$, m_a , n_a , p_a and q_a are four positive odd numbers. $m_a > n_a$, and $p_a < q_a$. For the design gain, $\alpha_a > 0$ and $\beta_a > 0$. $\mathbf{K}_h(t) = [\hat{K}_{h,1}(t), \hat{K}_{h,2}(t)]^T$ is the adaptive gain vector and is updated according to the adaptive law as follows:

$$\dot{\hat{K}}_{h,i}(t) = \rho_{2a} |s_{a,i}| - \rho_{1a} \hat{K}_{h,i} \quad (29)$$

Up to now, the disturbance observer for angle loop is summarized as

$$\begin{cases}
 \tilde{z}_a = z_a - e_a \\
 \dot{\tilde{z}}_a = \bar{F}_a + B_a \omega - \tilde{z}_{a,\text{nom}} + v_a \\
 \tilde{z}_{a,\text{nom}} = 2\beta_{\text{nom}} \sqrt{\arctan(\tilde{z}_a)} (I_2 + \tilde{z}_a^2) \text{sgn}(\tilde{z}_a) \\
 s_a = \tilde{z}_a(t) - \tilde{z}_a(0) + \int_0^t \tilde{z}_{a,\text{nom}} d\tau \\
 v_a = -\alpha_a \lceil s_a \rceil^{n_a} - \beta_a \lceil s_a \rceil^{q_a} - \hat{K}_h(t) \text{sgn}(s_a) \\
 \dot{\hat{K}}_{h,i}(t) = \rho_{2a} |s_{a,i}| - \rho_{1a} \hat{K}_{h,i}
 \end{cases} \quad (30)$$

Theorem 1: By considering the angular loop error system of the SGGP described by Eq. (21) and utilizing the designed disturbance observers in Eq. (30), the observer error tends to the origin in a fixed time, and the upper bound of the settling time is bounded by

$$T \leq T_{\max} = \frac{1}{2 \frac{p_a+q_a}{2q_a} \beta_a \Xi \left(\frac{q_a-p_a}{2q_a} \right)} + \frac{1}{2 \frac{m_a+n_a}{2n_a} \alpha_a \Xi \left(\frac{m_a-n_a}{2n_a} \right)} \quad (31)$$

Proof: The proof is given in Appendix. A.

3.2 Angle loop control command design based on the high-order fully actuated system approach

By considering B_a in Eq. (22) and calculating its determinant, the following can be obtained.

$$\begin{aligned}
 \det(B_a) &= \begin{vmatrix} 1 & -\cos \alpha \tan \beta \tan \vartheta + \sin \alpha \tan \beta \\ 0 & \sin \alpha \tan \vartheta + \cos \alpha \end{vmatrix} \\
 &= \cos(\vartheta - \alpha) / \cos \vartheta
 \end{aligned} \quad (32)$$

Because $\theta \approx \vartheta - \alpha$, $\det(B_a) = \frac{\cos \theta}{\cos \vartheta}$. When $\vartheta = \pm \frac{\pi}{2}$, singular problems appear. However, in the

whole midcourse flight process of the SGGP, the flight path angle and pitch angle satisfy two conditions:

$\theta \in \left(-\frac{\pi}{2}, \frac{\pi}{2} \right)$ and $\vartheta \in \left(-\frac{\pi}{2}, \frac{\pi}{2} \right)$. Therefore, the matrix B_a is invertible, and the error system in Eq. (22)

is fully actuated [36].

According to the definition, vector $x_a^{(0\Box 1)} = [x_a, \dot{x}_a]^T$ and coefficient matrix $K_a^{0\Box 1} = [K_{0a} \ K_{1a}]$. Then

the following virtual angular rate command $\omega_c = [\omega_{c1}, \omega_{c2}]^T$ is designed based on the high-order fully actuated system approach.

$$\begin{cases}
 \omega_c = -B_a^{-1} (\omega_{c,\text{in}} + \omega_c^*) \\
 \omega_c^* = \bar{F}_a + v_a - u_{\text{ex},1}
 \end{cases} \quad (33)$$

where $u_{\text{ex},1}$ is some external signal and $\omega_{c,\text{in}}$ is the PI feedback control law and expressed as

$$\omega_{c,\text{in}} = K_{1a}(x_a, \dot{x}_a) \dot{x}_a + K_{0a}(x_a, \dot{x}_a) x_a \quad (34)$$

where $K_{0a}(x_a, \dot{x}_a) \in \mathbf{R}^{2 \times 2}$ and $K_{1a}(x_a, \dot{x}_a) \in \mathbf{R}^{2 \times 2}$ are feedback gains vector and the rule for parameter selection will be presented later. By combining the fully actuated system and control law Eq. (33), one has

$$\ddot{\mathbf{x}}_a + K_{1a}(\mathbf{x}_a, \dot{\mathbf{x}}_a)\dot{\mathbf{x}}_a + K_{0a}(\mathbf{x}_a, \dot{\mathbf{x}}_a)\mathbf{x}_a = \mathbf{h}_a + \mathbf{u}_{\text{ex},1} \quad (35)$$

where $\mathbf{h}_a = \Delta \mathbf{d}_1 - \mathbf{v}_a$ is the tracking error of disturbance. The error will converge to a small neighborhood in a fixed time. When the external signal $\mathbf{u}_{\text{ex},1}$ is removed, Eq. (35) can be rewritten as follows:

$$\dot{\mathbf{x}}_a^{(0-1)} = \Phi(K_{0a \square 1a})\mathbf{x}_a^{(0-1)} + \begin{bmatrix} 0_{2 \times 1} \\ \mathbf{h}_a \end{bmatrix} \quad (36)$$

where $\Phi(K_{0a \square 1a}) = \begin{bmatrix} 0_{2 \times 2} & I_{2 \times 2} \\ -K_{0a} & -K_{1a} \end{bmatrix}$. Then, the problem is converted to design a matrix $K_{0a \square 1a}$ such that

$\Phi(K_{0a \square 1a})$ is stable.

Theorem 2: The closed-loop control system, which is composed of the second-order fully actuated system in Eq. (22), disturbance observer, and control law (33), is ultimately uniformly bounded, and the trajectory of the fully actuated system converges to the following neighborhood.

$$\Theta_a = \left\{ \mathbf{x}_a^{(0 \square 1)} \mid \left(\mathbf{x}_a^{(0 \square 1)} \right)^T P(A_{01}) \mathbf{x}_a^{(0 \square 1)} \leq \frac{K_a}{C_a} \right\}$$

Proof: The proof is given in the Appendix. B.

3.3. Control command design of an angular rate loop based on the high-order fully actuated system approach

Similar to the definition method in the above section, the vector $\sigma_\omega^{(0 \square 1)} = [\mathbf{x}_a, \dot{\mathbf{x}}_a]^T$ and the coefficient matrix $K_\omega^{0 \square 1} = [K_{0\omega} K_{1\omega}]$. The angular rate loop should track the virtual control law ω_c , so the tracking error is defined as

$$\mathbf{e}_\omega = \omega - \omega_c \quad (37)$$

Its derivative with respect to time is calculated as

$$\dot{\mathbf{e}}_\omega = \dot{\omega} - \dot{\omega}_c = \mathbf{F}_\omega + \mathbf{B}_\omega \delta + \Delta \mathbf{d}_2 - \dot{\omega}_c \quad (38)$$

First, a disturbance observer is designed to reconstruct the disturbance $\Delta \mathbf{d}_2$, and it has the same form as proposed in the angle loop design, which is constructed as

$$\begin{cases} \tilde{z}_\omega = z_\omega - \mathbf{e}_\omega \\ \dot{\tilde{z}}_\omega = \bar{\mathbf{F}}_\omega + \mathbf{B}_\omega \delta - \tilde{z}_{\omega, \text{nom}} + \mathbf{v}_\omega \\ \tilde{z}_{\omega, \text{nom}} = 2\beta_{\text{nom}} \sqrt{\arctan(\tilde{z}_\omega)} (\mathbf{I}_2 + \tilde{z}_\omega^2) \text{sgn}(\tilde{z}_\omega) \\ s_\omega = \tilde{z}_\omega(t) - \tilde{z}_\omega(0) + \int_0^t \tilde{z}_{\omega, \text{nom}} d\tau \\ \mathbf{v}_\omega = -\alpha_\omega |s_\omega|^{\frac{m_\omega}{n_\omega}} - \beta_\omega |s_\omega|^{\frac{p_\omega}{q_\omega}} - \hat{\mathbf{K}}_\omega(t) \text{sgn}(s_\omega) \\ \dot{\hat{\mathbf{K}}}_{\omega, i}(t) = \rho_{2\omega} |s_{\omega, i}| - \rho_{1\omega} \hat{\mathbf{K}}_{\omega, i} \end{cases} \quad (39)$$

Similarly, it is defined that $\sigma_\omega = \int_0^t \mathbf{e}_\omega d\tau$, and by calculating its second derivative corresponding to time, it is concluded that

$$\ddot{\sigma}_\omega = \mathbf{F}_\omega + \mathbf{B}_\omega \delta + \Delta \mathbf{d}_2 - \dot{\omega}_c = \underbrace{(\mathbf{F}_\omega - \dot{\omega}_c)}_{\bar{\mathbf{F}}_\omega} + \mathbf{B}_\omega \delta + \Delta \mathbf{d}_2 \quad (40)$$

where

$$\bar{\mathbf{F}}_\omega = \begin{bmatrix} a_{24}\alpha + a_{22}\omega_z + c_1\omega_y - \omega_y^2 \tan \vartheta - \omega_{c1} \\ b_{24}\beta + b_{22}\omega_y - c_2\omega_z + \omega_z\omega_y \tan \vartheta - \omega_{c2} \end{bmatrix}, \mathbf{B}_\omega = \begin{bmatrix} a_{25} & 0 \\ 0 & b_{25} \end{bmatrix} \quad (41)$$

The matrix \mathbf{B}_ω satisfies

$$\det(\mathbf{B}_\omega) \neq 0 \quad (42)$$

Therefore, system (40) is fully actuated. Based on high-order fully actuated control theory, the canard command is designed as follows.

$$\begin{cases} \delta = -\mathbf{B}_\omega^{-1}(\dot{\delta}_{\text{in}} + \delta^*) \\ \delta^* = \bar{\mathbf{F}}_\omega + \mathbf{h}_\omega - \mathbf{u}_{\text{ex},2} \end{cases} \quad (43)$$

Similar to Eq. (34), $\mathbf{u}_{\text{ex},2}$ refer to some external signal and the following PI feedback control law is adopted as

$$\delta_{\text{in}} = K_{1\omega}(\sigma_\omega, \dot{\sigma}_\omega)\dot{\sigma}_\omega + K_{0\omega}(\sigma_\omega, \dot{\sigma}_\omega)\sigma_\omega \quad (44)$$

where $K_{0\omega}(\sigma_\omega, \dot{\sigma}_\omega) \in \mathbf{R}^{2 \times 2}$ and $K_{1\omega}(\sigma_\omega, \dot{\sigma}_\omega) \in \mathbf{R}^{2 \times 2}$ are feedback gain vectors. By combining the second-order fully actuated system in Eq. (40) and control law in Eq. (43), the following can be obtained.

$$\ddot{\sigma}_\omega + K_{1\omega}(\sigma_\omega, \dot{\sigma}_\omega)\dot{\sigma}_\omega + K_{0\omega}(\sigma_\omega, \dot{\sigma}_\omega)\sigma_\omega = \mathbf{h}_\omega + \mathbf{u}_{\text{ex},2} \quad (45)$$

where \mathbf{h}_ω represents the tracking errors in the disturbance observer and the estimation error converges to a small neighborhood in a fixed time. When the external signal $\mathbf{u}_{\text{ex},2}$ is removed, system (45) can be reconstructed as follows:

$$\dot{\sigma}_\omega^{(0\Box 1)} = \Phi(K_{0\omega\Box 1\omega})\sigma_\omega^{(0\Box 1)} + \begin{bmatrix} 0_{2 \times 1} \\ \mathbf{h}_\omega \end{bmatrix} \quad (46)$$

where $\Phi(K_{0\omega\Box 1\omega}) = \begin{bmatrix} 0_{2 \times 2} & I_{2 \times 2} \\ -K_{0\omega} & -K_{1\omega} \end{bmatrix}$. Then, the problem is also converted to design a matrix $K_{0\omega\Box 1\omega}$

such that $\Phi(K_{0\omega\Box 1\omega})$ is stable.

Theorem 3: The closed-loop system, which is composed of the fully actuated system in (40), observer in (39), and control law in (43), is ultimately uniformly bounded, and the trajectory of the fully actuated system converges to the following neighborhood.

$$\Theta_\omega = \left\{ \sigma_\omega^{(0\Box 1)} \mid \left(\sigma_\omega^{(0\Box 1)} \right)^T P(A_{0\Box 1}) \sigma_\omega^{(0\Box 1)} \leq \frac{K_w}{C_\omega} \right\} \quad (47)$$

Proof: The proof is similar to the proof of theorem 2, which is omitted here.

Remark 2. Inspired by the fixed-time stable theory, an improved fixed-time converged low pass filter (FxLPF) proposed in Ref. [37] is given below to acquire the differential signal in this paper

$$\tau_1 \dot{x}_d = c_1 [x_c - x_d]^{\beta_1} + c_2 [x_c - x_d]^{\beta_2}, x_c(0) = x_d(0) \quad (48)$$

where x_c and x_d denote the input and output signals of FxLPF, respectively. In addition, $\tau_1 > 0$, $c_1 > 0$, $c_2 > 0$, $\beta_1 < 1$ and $\beta_2 > 1$ are design parameters.

The tracking error signal is defined as $\tilde{x}_c = x_c - x_d$. Its derivative with respect to time is calculated as

$$\dot{\tilde{x}}_c = -\frac{c_1}{\tau_1}[\tilde{x}_c]^{\beta_1} - \frac{c_2}{\tau_1}[\tilde{x}_c]^{\beta_2} + \dot{x}_c \quad (49)$$

Here, \dot{x}_c is regarded as a bounded disturbance that satisfies $|\dot{x}_c| < \bar{x}_c$, where $\bar{x}_c > 0$ is a constant.

Recalling lemma 1, the tracking error converges to the following domain Ω_τ in a fixed time $T_{\tau s}$.

$$\Omega_\tau = \left\{ \lim_{t \rightarrow T_{\tau s}} \tilde{x}_c \mid \tilde{x}_c \leq \min \left\{ \left(\frac{\tau_1 \bar{x}_c}{c_1(1-\phi_\tau)} \right)^{\frac{1}{\beta_1}}, \left(\frac{\tau_1 \bar{x}_c}{c_2(1-\phi_\tau)} \right)^{\frac{1}{\beta_2}} \right\} \right\} \quad (50)$$

where $\phi_\tau \in (0,1)$ and the settling time $T_{\tau s}$ is bounded by

$$T_{\tau s} \leq T_{\tau s, \max} = \frac{\tau_1}{c_1 \phi_\tau (1-\beta_1)} \quad (51)$$

Therefore, the tracking error of FxLPF is practically fixed-time stable.

3.4. Selection of the coefficient matrix

Proposition 2: For an arbitrary matrix $Q \in \mathbf{R}^{nr \times nr}$, the coefficient matrix $K^{0\Box 1}$ and nonsingular matrix $V \in \mathbf{R}^{nr \times nr}$ satisfy

$$\Phi(K^{0\Box 1}) = VQV^{-1} \quad (52)$$

where

$$K^{0\Box 1} = -ZQ^n V^{-1}(Z, F) \quad (53)$$

$$V = V(Z, F) = \begin{bmatrix} Z \\ ZF \\ \dots \\ ZF^{n-1} \end{bmatrix} \quad (54)$$

where $Z \in \mathbf{R}^{r \times nr}$ is a random coefficient matrix that satisfies

$$\det V(Z, F) \neq 0 \quad (55)$$

The following gain selection method is created to realize the fast tracking of the angle loop. The closed-loop poles $s_1 = s_2 = -\omega_{n1}$ and $s_3, s_4 = -\omega_{n2} \pm j\xi_n$ are considered. Here, ω_n represents the natural frequency of the system, and ξ_n represents damping. Letting $0 < \omega_{n1} < \omega_{n2}$, s_1, s_2 are the dominant poles. The gain matrix can be expressed as follows.

$$F = \text{blockdiag} \left(\begin{array}{cc} -\omega_{n1} I_{2 \times 2} & 0_{2 \times 2} \\ 0_{2 \times 2} & \begin{bmatrix} -\omega_{n2} & 3\omega_{n2}^2 / 4 + \xi_n^2 \\ 1 & -\omega_{n2} \end{bmatrix} \end{array} \right) \quad (56)$$

Furthermore,

$$F^2 = \begin{bmatrix} \omega_{n1}^2 I_{2 \times 2} & 0 \\ 0 & \begin{bmatrix} 7\omega_{n2}^2 / 4 + \xi_n^2 & -2\omega_{n2}(3\omega_{n2}^2 / 4 + \xi_n^2) \\ -2\omega_{n2} & 7\omega_{n2}^2 / 4 + \xi_n^2 \end{bmatrix} \end{bmatrix} \quad (57)$$

It is defined that $Z = [I_{2 \times 2} \ I_{2 \times 2}]$, and then,

$$V = \begin{bmatrix} I_{2 \times 2} & I_{2 \times 2} \\ -\omega_{n1} I_{2 \times 2} & \begin{bmatrix} -\omega_{n2} & 3\omega_{n2}^2 / 4 + \xi_n^2 \\ 1 & -\omega_{n2} \end{bmatrix} \end{bmatrix} \quad (58)$$

Its inverse matrix is expressed as

$$V^{-1} = \frac{1}{\Lambda} \begin{bmatrix} \omega_{n1} - \omega_{n2} + \Lambda & -3\omega_{n2}^2 / 4 - \xi_n^2 & \omega_{n2}^2 - \omega_{n1} & 3\omega_{n2}^2 / 4 + \xi_n^2 \\ -1 & \omega_{n1} - \omega_{n2} + \Lambda & 1 & \omega_{n2} - \omega_{n1} \\ \omega_{n1}(\omega_{n1} - \omega_{n2}) & -\omega_{n1}(3\omega_{n2}^2 / 4 + \xi_n^2) & \omega_{n1} - \omega_{n2} & -3\omega_{n2}^2 / 4 - \xi_n^2 \\ -\omega_{n1} & \omega_{n1}(\omega_{n1} - \omega_{n2}) & -1 & \omega_{n1} - \omega_{n2} \end{bmatrix} \quad (59)$$

where $\Lambda = \det V(Z, F) = \omega_{n1}^2 - 2\omega_{n1}\omega_{n2} + \omega_{n2}^2 / 4 - \xi_n^2 \neq 0$. On this basis, the gain matrix in control law (34)

can be expressed as follows.

$$K_{0a \square 1a} = -ZF^2V^{-1} = [K_{0a} \ K_{1a}] \quad (60)$$

where

$$K_{0a} = \frac{1}{\Lambda} \begin{bmatrix} a_{a01} & a_{a02} \\ a_{a03} & a_{a04} \end{bmatrix}, K_{1a} = \frac{1}{\Lambda} \begin{bmatrix} a_{a11} & a_{a12} \\ a_{a13} & a_{a14} \end{bmatrix} \quad (61)$$

and the following holds.

$$\begin{cases} a_{a01} = a_{a04} = \omega_{n1}^2(\omega_{n1} - \omega_{n2} + \Lambda) + \omega_{n1}(\omega_{n1} - \omega_{n2})(7\omega_{n2}^2 / 4 + \xi_n^2) + 2\omega_{n1}\omega_{n2}(3\omega_{n2}^2 / 4 + \xi_n^2) \\ a_{a02} = \omega_{n1}(3\omega_{n2}^2 / 4 + \xi_n^2)(\omega_{n2}^2 / 4 - \omega_{n1} - 2\omega_{n1}\omega_{n2} - \xi_n^2) \\ a_{a03} = -\omega_{n1}^2 - 2\omega_{n1}\omega_{n2}(\omega_{n1} - \omega_{n2}) - \omega_{n1}(7\omega_{n2}^2 / 4 + \xi_n^2) \\ a_{a11} = a_{a14} = -\omega_{n1}^2(\omega_{n1} - \omega_{n2}) + (\omega_{n1} - \omega_{n2})(7\omega_{n2}^2 / 4 + \xi_n^2) + 2\omega_{n2}(3\omega_{n2}^2 / 4 + \xi_n^2) \\ a_{a12} = (3\omega_{n2}^2 / 4 + \xi_n^2)(\omega_{n1}^2 + \omega_{n2}^2 / 4 - 2\omega_{n2}\omega_{n1} - \xi_n^2) \\ a_{a13} = \omega_{n1}^2 - 2\omega_{n2}(\omega_{n1} - \omega_{n2}) - 7\omega_{n2}^2 / 4 - \xi_n^2 \end{cases} \quad (62)$$

The parametric approach of the gain matrix in angle loop control law (34) and angular rate loop control law (44) is the same as that in Eqs. (52)–(62).

4. Case study

This section includes numerous numerical simulations based on the designed attitude autopilot to verify the effectiveness of the proposed control scheme. The initial flight parameters of an SGGP are given in Table 1.

Table 1

Gliding flight parameters of the SGGP.

Parameters	Value	Parameters	Value
m/kg	53.0	$m_z^{\bar{\omega}_z}$	-2.0
$V(\text{m}\cdot\text{s}^{-1})$	280	$m_z^{\delta_z}$	4.2211
S/m^2	0.019	m_y^{β}	-0.241
L/m	1.1	$m_y^{\bar{\omega}_y}$	-10.5312
$\theta/(\text{rad})$	0.017	$m_y^{\delta_y}$	4.2211
c_y^{α}	0.259	J_x	4.9969
c_z^{β}	0.2421	J_y	4.9969
m_z^{α}	-4.4276	J_z	0.0033

The user-defined parameters are given in Table 2.

Table 2

Parameters of the proposed controller.

Parameters	Value	Parameters	Value
ω_{n1}, ω_{n2}	5	P_a, P_{ω}	7
ξ_n	0.7	q_a, q_{ω}	9
α_a, β_a	2	$\alpha_{\omega}, \beta_{\omega}$	2
$\hat{K}_h(0), \hat{K}_{\omega}(0)$	5	c_1, c_2	1
m_a, m_{ω}	5	ρ_{1a}, ρ_{2a}	0.001,10
n_a, n_{ω}	3	$\rho_{1\omega}, \rho_{2\omega}$	0.001,10

4.1. Attitude tracking test

First, the following functions are used as the reference signal.

$$\begin{cases} \alpha_{\text{ref}} = 5(\cos(2t) \cdot \sin(0.8t)) + 2(^{\circ}) \\ \beta_{\text{ref}} = 5(\sin(2t) \cdot \cos(0.6t)) - 4(^{\circ}) \end{cases} \quad (63)$$

The initial value of the angle is set as $\boldsymbol{\Omega}(0)=[0,0]^T$, and the initial value of the angular rate is $\boldsymbol{\omega}(0)=[0,0]^T$. As depicted in Fig. 3(a), despite aerodynamic uncertainties and external disturbances, both the angle of attack and sideslip angle achieve reference signal tracking within 0.5 s. Fig. 3(b) illustrates the variation curve of the angular rates, revealing a smoothly designed virtual control law ω_c . Furthermore, under the action of the designed canard angle, ω_z and ω_y rapidly and accurately track the virtual control signal, accomplished within 0.5 s.

As portrayed in Fig. 3(c), the canard commands and canard deflections are presented. Simulation results confirm that the composite fully actuated controller ensures smooth deflection command and actual deflection of canards, meeting the input saturation limits. As shown in Fig. 3(d), due to the use of integral signals in the design of the controller, the steady-state error is effectively reduced so that the designed controller can ensure the tracking performance of the closed-loop system.

Depicted in Figs. 3(e) and 3(f), the disturbance observer precisely estimates the total disturbance for

both the angle loop and angular rate loop. Applying the estimated value to feedforward compensation effectively reduces the burden of gain feedback in controller selection. Fig. 3(g) presents the variation curve of the adaptive gain in the disturbance observer. As the change curve shows, the adaptive gain decreases as the estimation error decreases. As a result, the chattering problem in conventional sliding mode control is overcome. Compared with the adaptive sliding mode control law used in Ref. [38], the adaptive sliding mode control law used in this paper achieves an accurate estimation of the disturbance and ensures the boundedness of the adaptive parameters.

Fig. 3(h) shows the variation curve of the integral sliding mode variable. One can observe that the designed integral sliding mode variable remains on the sliding mode surface from the initial moment. The sliding mode variable enters the sliding motion at the initial moment and maintains the sliding motion in the subsequent control process. The singularity problem is solved by eliminating the reaching phase, and the estimation errors converge to origin within a fixed-time.

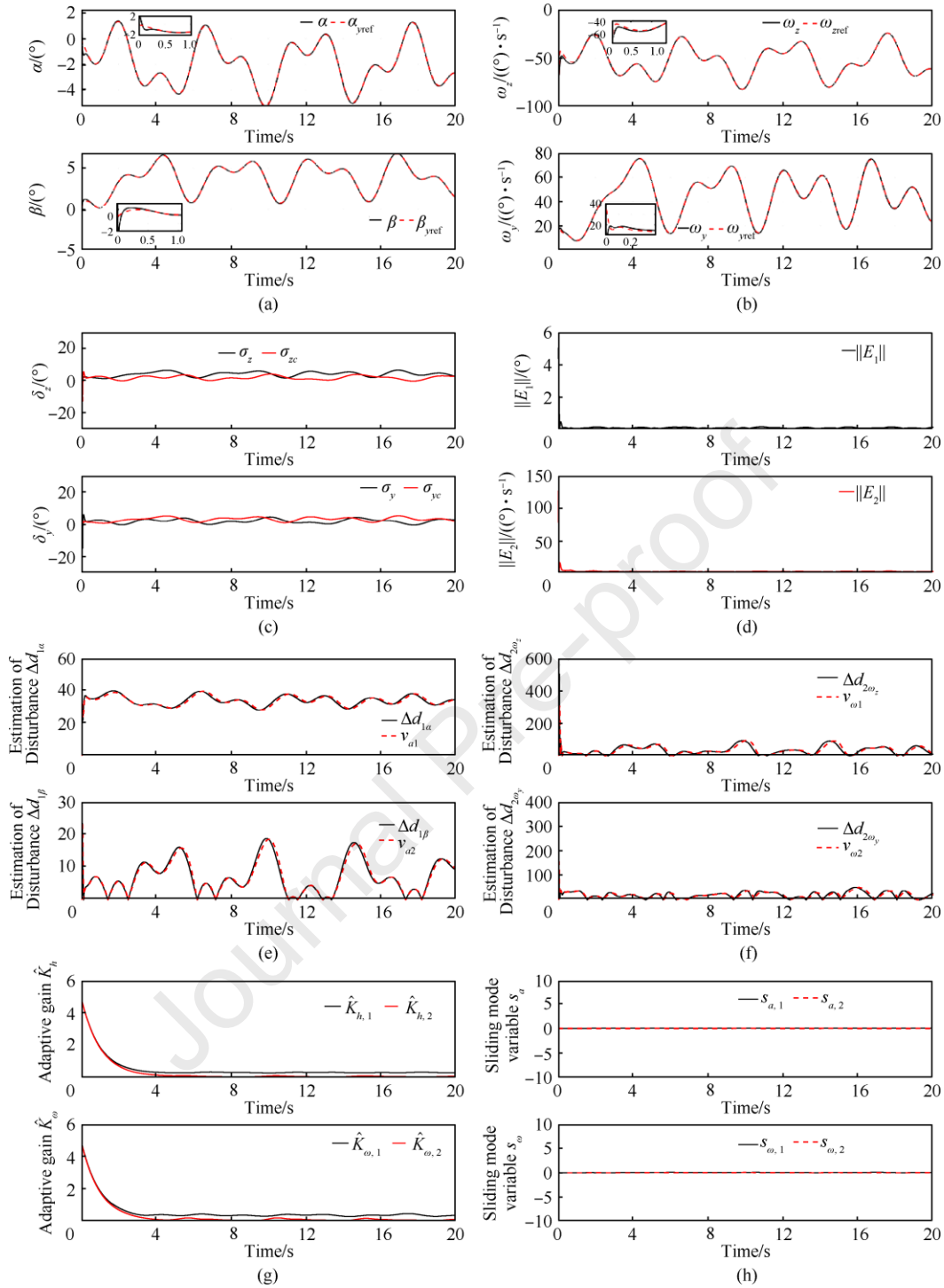


Fig. 3. Simulation results of numerical example #1: (a) Attitude angles; (b) Angular rates; (c) Deflection angle of canards; (d) Bound of the tracking error; (e) Estimation of angle loop disturbance; (f) Estimation of angular rate loop disturbance; (g) Adaptive gains; (h) Sliding mode variables.

Furthermore, the square signal with an amplitude of 0.3 rad is used as the reference signal for numerical simulation. Figs. 4(a) and 4(b) depict the angles and angular rates. Using the proposed autopilot design, both angles and angular rates efficiently track the given reference signal. Fig. 4(c) illustrates canard commands and actual canard deflections. Large initial tracking errors cause significant

canard deflections for a quick projectile response. As errors reduce, the deflections become minor to counter disturbances. Notably, sharp changes in the reference signal lead to abrupt canard deflections, yet within physical input limit. Fig. 4(d) display the norm bound of the tracking error, which converges rapidly. Figs. 4(e) and 4(f) given the estimation of disturbance in angle and angular loop. One can see that the designed observer can achieve fast and accurate tracking of the total disturbances. Therefore, the burden of feedback controller gain selection is reduced. From the simulation results given in Fig. 4(g), one can see that the boundedness of the adaptive parameters is guaranteed. Fig. 4(h) shows the change curve of the integral sliding mode variable. According to the simulation diagram, the designed integral sliding mode variable maintains the sliding motion at the beginning of the control process.

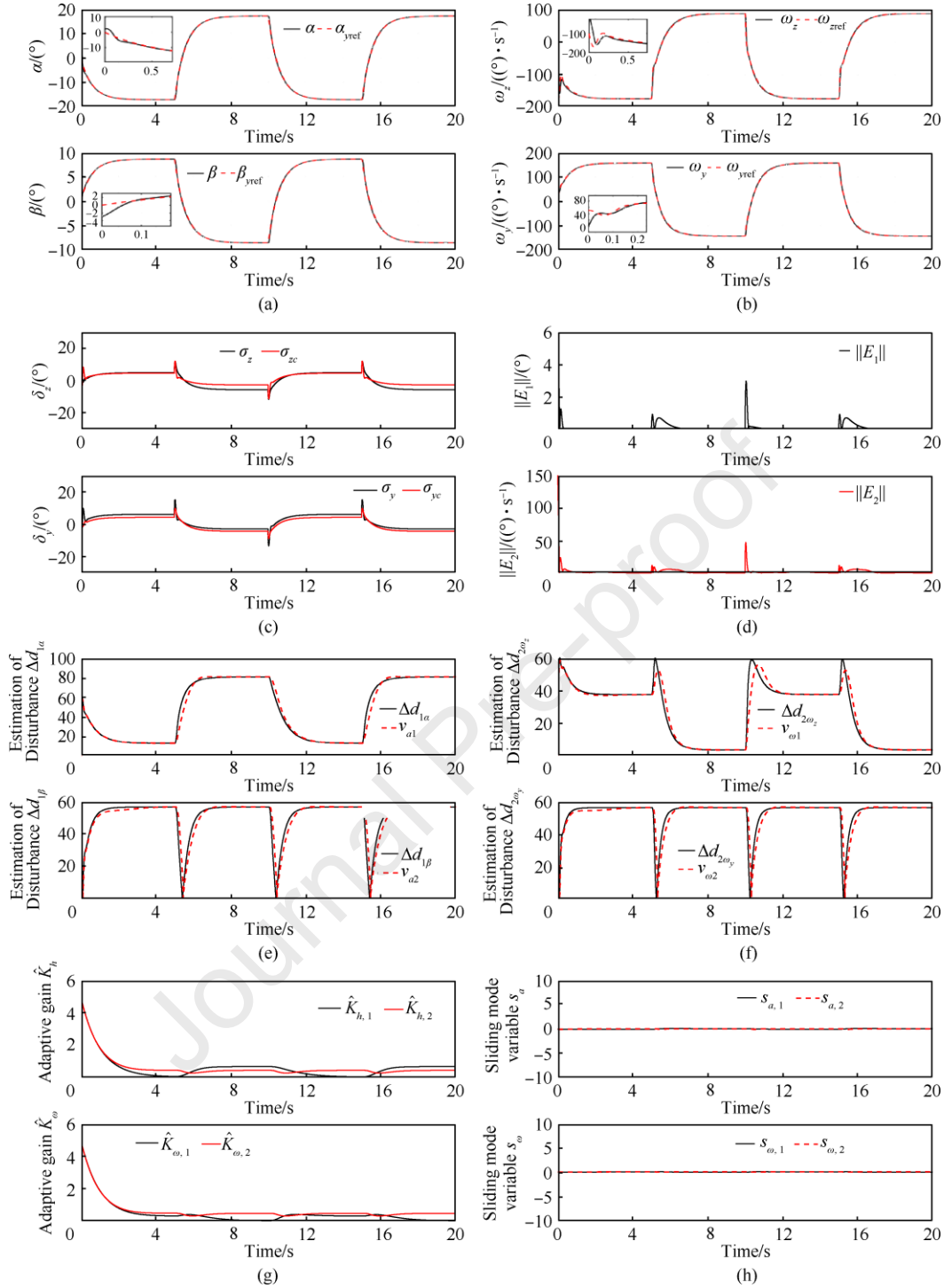


Fig. 4. Simulation result of numerical example #2: (a) Attitude angles; (b) Angular rates; (c) Canard deflection angles; (d) Bound of the tracking error; (e) Estimation of angle loop disturbance; (f) Estimation of angular rate loop disturbance; (g) Adaptive gains; (h) Sliding mode variables.

4.2. Comparison with existing control laws

To demonstrate the effectiveness and superiority of the designed controller, the designed method is compared with the trajectory linearization control-based sliding mode controller (TLC-SMC) [39] and trajectory linearization control-based integral sliding mode controller (TLC-ISMC) [40]. A square signal

serves as the reference signal throughout. Figs. 5(a) and 5(b) show the tracking curves of the angles and angular rates, respectively. While all three controllers track the given signal precisely, according to the enlarged figures, the angles in the TLC-SMC and TLC-ISMC control schemes are subject to the chattering phenomenon. In contrast, the angle profiles of the proposed controller are smooth. Reviewing the angular rate curve in Fig. 5(b), the chattering phenomenon under the SMC-based controllers is more prominent. Figs. 5(c) and 5(d) depict the deflection angles, and it's evident that the autopilot based on HOFAS is significantly smoother. The requirements for the actuator frequency are reduced, which is conducive to practical applications. Fig. 5(e) shows the norm of tracking error, and the sliding mode controller can achieve rapid convergence of the errors, their cannot overcome the inherent chattering problem of sliding mode control. The index function $J = \int_0^t \delta_z^2 + \delta_y^2 d\tau$ is chosen to illustrate the control energy consumption, and the diagram is shown in Fig. 5(f). This diagram suggests that, compared with the high-frequency sliding mode control, the controller designed in this paper has a more significant advantage in energy consumption.

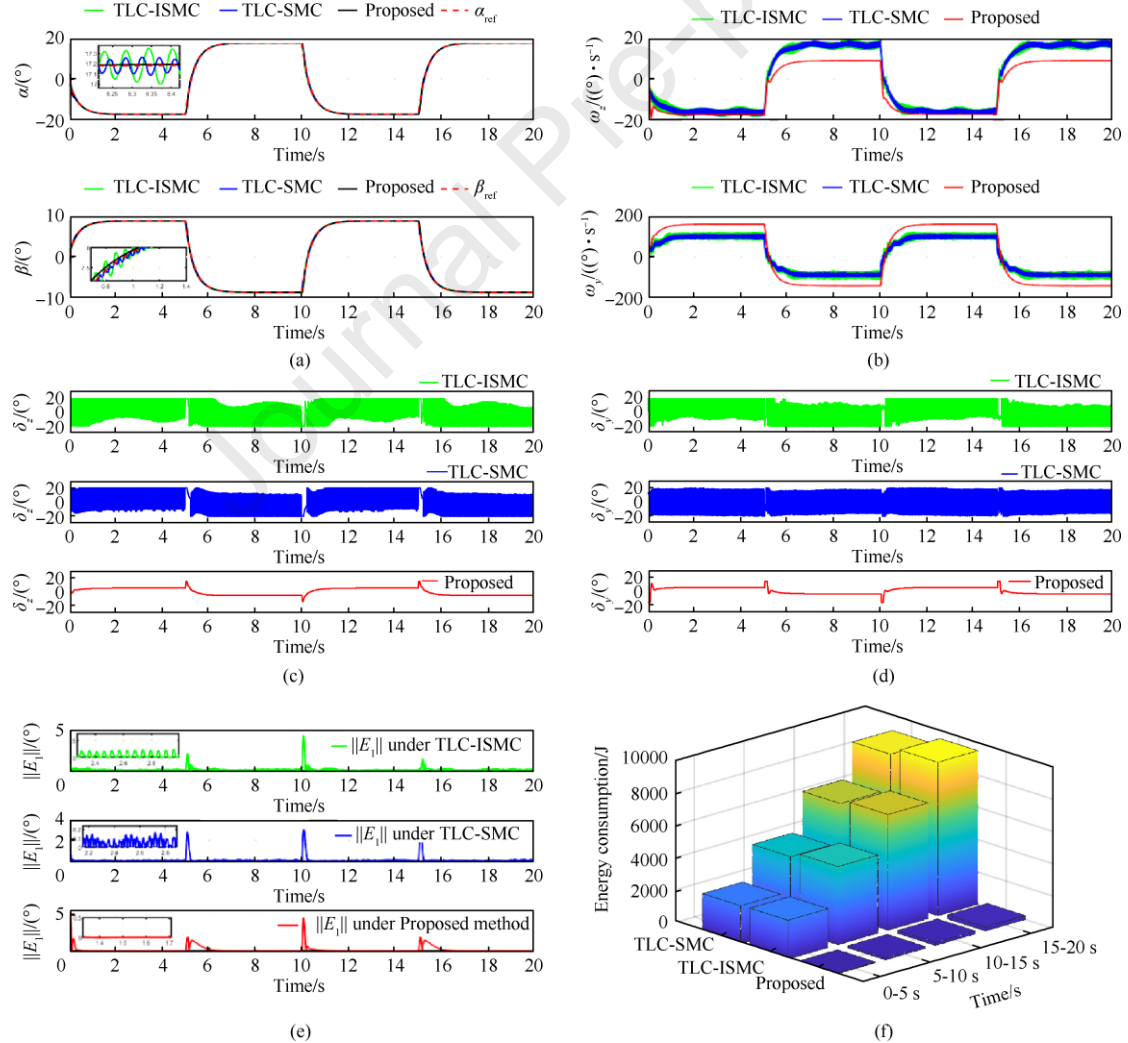


Fig. 5. Comparative experiment: (a) Attitude angles; (b) Angular rates; (c) Canard deflection angle; (d) Canard deflection angle; (e) Bound of the tracking error; (f) Energy consumption.

4.3. Monte-Carlo test

To verify the robustness of the designed control method against aerodynamic uncertainties and the convergence rates of different initial errors, 100 Monte Carlo simulations are carried out. The initial angle deviation is $\Omega \sim N(0, R)$, where $R \in (2,3)^\circ$, and the aerodynamic parameters positively deviate by 60%. Figs. 6(a) and 6(b) show the change curves of the angles and angular rates. Despite the presence of aerodynamic uncertainties and substantial initial disturbances, the simulation results indicate that both angles and angular rates consistently track the reference signals. As illustrated in Fig. 6(c), when faced with large initial disturbance, the canard initially deflects significantly for fast error convergence. As the error reduces, its deflection becomes smaller. Fig. 6(d) presents the variation curve of the norm of tracking error. According to the simulation diagram, the designed controller can ensure the fast and smooth convergence of the error even when the initial error is large. The designed attitude autopilot's robustness, rapidity, and superiority are verified.

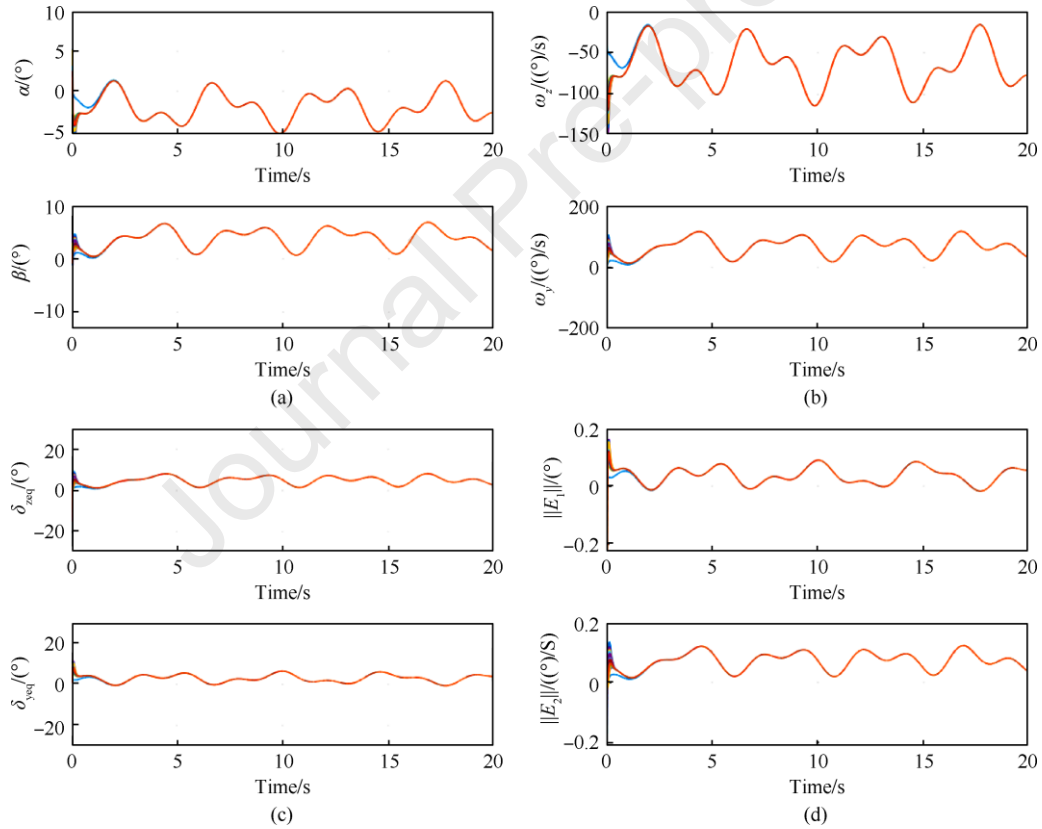


Fig. 6. Monte-Carlo experiment: (a) Attitude angles; (b) Angular rates; (c) Canard deflections; (d) Upper bound of the tracking errors.

5. Conclusions

In this research, a robust attitude autopilot was developed for a dual-channel controlled SGPP during its midcourse flight phase, addressing model uncertainties and external disturbance. A fixed-time disturbance observer is proposed based on the modified adaptation law and integral sliding mode

technique. The total disturbances are estimated by the proposed observer without prior information, which is crucial in practical application. For attitude tracking control, a complete second-order nonlinear model with fully actuated characteristics for the SGPP attitude dynamics is developed. Combined with the HOFAS approach and parametric approach, the developed nonlinear system is transformed into a constant linear system with the desired eigenstructure. Moreover, the performance of the proposed attitude autopilot is evaluated with multiple numerical simulation studies, and the superiority is demonstrated by comparison with existing attitude control schemes.

Appendix. A

A Lyapunov function is defined below.

$$V_1 = \frac{1}{2} s_a^T s_a + \frac{1}{2\rho_2} \sum_{i=1}^2 \tilde{K}_{h,i}^2 \quad (64)$$

where $\tilde{K}_{h,i} = \bar{K}_{h,i} - \hat{K}_{h,i}$. $\bar{K}_{h,i}$ represents the estimated upper bound of the adaptive parameters. The first derivative corresponding to time is obtained in equation (30) and proposition 1, after substitution, one has

$$\begin{aligned} \dot{V}_1 &= \sum_{i=1}^2 s_{a,i} \dot{s}_{a,i} - \frac{1}{\rho_2} \sum_{i=1}^2 \tilde{K}_{h,i} \dot{\hat{K}}_{h,i} \\ &= \sum_{i=1}^2 \left(s_{a,i} h_i - \alpha_a |s_{a,i}|^{\frac{m_a+n_a}{n_a}} - \beta_a |s_{a,i}|^{\frac{p_a+q_a}{q_a}} - \hat{K}_{h,i} \cdot |s_{a,i}| \right) - \frac{1}{\rho_2} \sum_{i=1}^2 \tilde{K}_{h,i} (\rho_{2a} |s_{a,i}| - \rho_{1a} \hat{K}_{h,i}) \\ &\leq \sum_{i=1}^2 \left(|s_{a,i}| |\Delta h_i| - \alpha_a |s_{a,i}|^{\frac{m_a+n_a}{n_a}} - \beta_a |s_{a,i}|^{\frac{p_a+q_a}{q_a}} - \hat{K}_{h,i} \cdot |s_{a,i}| \right) - \frac{1}{\rho_2} \sum_{i=1}^2 \tilde{K}_{h,i} (\rho_{2a} |s_{a,i}| - \rho_{1a} \hat{K}_{h,i}) \\ &= \sum_{i=1}^2 \left(|s_{a,i}| |\Delta h_i| - \alpha_a |s_{a,i}|^{\frac{m_a+n_a}{n_a}} - \beta_a |s_{a,i}|^{\frac{p_a+q_a}{q_a}} - \bar{K}_{h,i} \cdot |s_{a,i}| \right) + \frac{\rho_{1a}}{\rho_{2a}} \sum_{i=1}^2 \tilde{K}_{h,i} \hat{K}_{h,i} \end{aligned} \quad (65)$$

By using Young's inequality, one has

$$\begin{aligned} \tilde{K}_{h,i} \hat{K}_{h,i} &= \tilde{K}_{h,i} (\bar{K}_{h,i} - \tilde{K}_{h,i}) = \tilde{K}_{h,i} \bar{K}_{h,i} - \tilde{K}_{h,i}^2 \\ &\leq \frac{1}{2} (\bar{K}_{h,i}^2 + \tilde{K}_{h,i}^2) - \tilde{K}_{h,i}^2 = \frac{1}{2} \bar{K}_{h,i}^2 - \frac{1}{2} \tilde{K}_{h,i}^2 \\ &\leq \frac{1}{2} \bar{K}_{h,i}^2 \end{aligned} \quad (66)$$

Furthermore, equation (65) can be scaled as follows:

$$\begin{aligned} \dot{V}_1 &\leq \sum_{i=1}^2 \left(-\alpha_a |s_{a,i}|^{\frac{m_a+n_a}{n_a}} - \beta_a |s_{a,i}|^{\frac{p_a+q_a}{q_a}} \right) + \frac{\rho_{1a}}{2\rho_{2a}} \sum_{i=1}^2 \bar{K}_{h,i}^2 \\ &= \sum_{i=1}^2 \left(\frac{\rho_{1a}}{4\rho_{2a}} \bar{K}_{h,i}^2 - \alpha_a |s_{a,i}|^{\frac{m_a+n_a}{n_a}} \right) + \sum_{i=1}^2 \left(\frac{\rho_{1a}}{4\rho_{2a}} \bar{K}_{h,i}^2 - \beta_a |s_{a,i}|^{\frac{p_a+q_a}{q_a}} \right) \\ \text{If } |s_{a,i}| > \max &\left\{ \left(\frac{\rho_{1a}}{4\alpha_a \rho_{2a}} \bar{K}_{h,i}^2 \right)^{\frac{n_a}{m_a+n_a}}, \left(\frac{\rho_{1a}}{4\beta_a \rho_{2a}} \bar{K}_{h,i}^2 \right)^{\frac{q_a}{p_a+q_a}} \right\}, \dot{V}_1 < 0. \text{ The observer closed-loop system} \end{aligned} \quad (67)$$

converges to the following adjustable neighborhood.

$$\Omega_v \square \left\{ s_{a,i} \parallel s_{a,i} \leq \max \left\{ \left(\frac{\rho_{1a}}{4\alpha_a \rho_{2a}} \bar{K}_{h,i}^2 \right)^{\frac{n_a}{m_a+n_a}}, \left(\frac{\rho_{1a}}{4\beta_a \rho_{2a}} \bar{K}_{h,i}^2 \right)^{\frac{q_a}{p_a+q_a}} \right\} \right\} \quad (68)$$

The sliding mode variables and adaptive gain of the observer system are both bounded. They are related as follows:

$$\begin{aligned} V_1^{\frac{m_a+n_a}{2n_a}} &= \left[\frac{1}{2} s_a^T s_a + \frac{1}{2\rho_{2a}} \sum_{i=1}^2 \bar{K}_{h,i}^2 \right]^{\frac{m_a+n_a}{2n_a}} \leq \left(\frac{1}{2} s_a^T s_a \right)^{\frac{m_a+n_a}{2n_a}} + \left(\frac{1}{2\rho_{2a}} \sum_{i=1}^2 \bar{K}_{h,i}^2 \right)^{\frac{m_a+n_a}{2n_a}} \\ &\Rightarrow \left(\frac{1}{2} s_a^T s_a \right)^{\frac{m_a+n_a}{2n_a}} \geq V_1^{\frac{m_a+n_a}{2n_a}} - \left(\frac{1}{2\rho_{2a}} \sum_{i=1}^2 \bar{K}_{h,i}^2 \right)^{\frac{m_a+n_a}{2n_a}} \end{aligned} \quad (69)$$

and

$$\begin{aligned} V_1^{\frac{p_a+q_a}{2q_a}} &= \left[\frac{1}{2} s_a^T s_a + \frac{1}{2\rho_{2a}} \sum_{i=1}^2 \bar{K}_{h,i}^2 \right]^{\frac{p_a+q_a}{2q_a}} \leq \left(\frac{1}{2} s_a^T s_a \right)^{\frac{p_a+q_a}{2q_a}} + \left(\frac{1}{2\rho_{2a}} \sum_{i=1}^2 \bar{K}_{h,i}^2 \right)^{\frac{p_a+q_a}{2q_a}} \\ &\Rightarrow \left(\frac{1}{2} s_a^T s_a \right)^{\frac{p_a+q_a}{2q_a}} \geq V_1^{\frac{p_a+q_a}{2q_a}} - \left(\frac{1}{2\rho_{2a}} \sum_{i=1}^2 \bar{K}_{h,i}^2 \right)^{\frac{p_a+q_a}{2q_a}} \end{aligned} \quad (70)$$

By combining the first equations in Eqs. (69), (70), and (67), one has

$$\begin{aligned} \dot{V}_1 &\leq -2^{\frac{m_a+n_a}{2n_a}} \alpha_a \left(\frac{1}{2} s_a^T s_a \right)^{\frac{m_a+n_a}{2n_a}} - 2^{\frac{p_a+q_a}{2q_a}} \beta_a \left(\frac{1}{2} s_a^T s_a \right)^{\frac{p_a+q_a}{2q_a}} + \frac{\rho_{1a}}{2\rho_{2a}} \sum_{i=1}^2 \bar{K}_{h,i}^2 \\ &\leq -2^{\frac{m_a+n_a}{2n_a}} \alpha_a \left(V_1^{\frac{m_a+n_a}{2n_a}} - \left(\frac{1}{2\rho_{2a}} \sum_{i=1}^2 \bar{K}_{h,i}^2 \right)^{\frac{m_a+n_a}{2n_a}} \right) - 2^{\frac{p_a+q_a}{2q_a}} \beta_a \left(V_1^{\frac{p_a+q_a}{2q_a}} - \left(\frac{1}{2\rho_{2a}} \sum_{i=1}^2 \bar{K}_{h,i}^2 \right)^{\frac{p_a+q_a}{2q_a}} \right) \\ &\quad + \frac{\rho_{1a}}{2\rho_{2a}} \sum_{i=1}^2 \bar{K}_{h,i}^2 \\ &= -2^{\frac{m_a+n_a}{2n_a}} \alpha_a V_1^{\frac{m_a+n_a}{2n_a}} - 2^{\frac{p_a+q_a}{2q_a}} \beta_a V_1^{\frac{p_a+q_a}{2q_a}} + \Theta_0 \end{aligned} \quad (71)$$

It can be seen from the previous analysis that the estimation errors and adaptive parameters are bounded. Therefore, it is further obtained from Lemma 1 that the observer closed-loop system is fixed-time stable, and the settling time is bounded as follows:

$$T \leq T_{\max} = \frac{1}{2^{\frac{p_a+q_a}{2q_a}} \beta_a \Xi \left(\frac{q_a - p_a}{2q_a} \right)} + \frac{1}{2^{\frac{m_a+n_a}{2n_a}} \alpha_a \Xi \left(\frac{m_a - n_a}{2n_a} \right)} \quad (72)$$

From the properties of ISMC, $\dot{s}_a=0$ from the initial time; then, the following can be obtained:

$$\dot{\tilde{z}}_a = 2\beta_{\text{nom}} \sqrt{\|\arctan(\tilde{z}_a)\|} \left(I_2 + \tilde{z}_a^2 \right) \text{sgn}(\tilde{z}_a) \quad (73)$$

Recalling Lemma 2, the estimation error converges to the origin in a fixed time, and the channel disturbance reconstruction can be realized. This completes the proof.

Appendix. B

A Lyapunov function is designed as follows:

$$V_a = \frac{1}{2} \left(\mathbf{x}_a^{(0\Box 1)} \right)^T P(A_{01}) \mathbf{x}_a^{(0\Box 1)} \quad (74)$$

By calculating its derivative and substituting it into the equation, the following is obtained:

$$\begin{aligned} \dot{V}_a &= \frac{1}{2} \left(\dot{\mathbf{x}}_a^{(0\sim 1)} \right)^T P(A_{0-1}) \mathbf{x}_a^{(0\sim 1)} + \frac{1}{2} \left(\mathbf{x}_a^{(0\sim 1)} \right)^T P(A_{0-1}) \dot{\mathbf{x}}_a^{(0\sim 1)} \\ &= \frac{1}{2} \left(\Phi(A_{0\sim 1}) \mathbf{x}_a^{(0\sim 1)} + \begin{bmatrix} 0_{2 \times 1} \\ \tilde{\mathbf{h}}_a \end{bmatrix} \right)^T P \mathbf{x}_a^{(0\sim 1)} + \frac{1}{2} \left(\mathbf{x}_a^{(0\sim 1)} \right)^T P \left(\Phi(K_{0a\sim 1a}) \mathbf{x}_a^{(0\sim 1)} + \begin{bmatrix} 0_{2 \times 1} \\ \tilde{\mathbf{h}}_a \end{bmatrix} \right) \\ &= \frac{1}{2} \left(\mathbf{x}_a^{(0\sim 1)} \right)^T \left(\Phi^T P + P \Phi \right) \left(\mathbf{x}_a^{(0\sim 1)} \right) + \left(\mathbf{x}_a^{(0\sim 1)} \right)^T P \begin{bmatrix} 0_{2 \times 1} \\ \tilde{\mathbf{h}}_a \end{bmatrix} \\ &\leq -\frac{\alpha}{2} \left(\mathbf{x}_a^{(0\sim 1)} \right)^T P \mathbf{x}_a^{(0\sim 1)} + \frac{\eta}{2} \mathbf{x}_a^{(0\sim 1)T} \mathbf{x}_a^{(0\sim 1)} + \frac{1}{2\eta} P_{L2} \tilde{\mathbf{h}}_a \\ &= -\frac{1}{2} \left(\mathbf{x}_a^{(0\sim 1)} \right)^T (\alpha P - \eta I) \mathbf{x}_a^{(0\sim 1)} + \frac{1}{2\eta} P_{L2} \tilde{\mathbf{h}}_a \\ &\leq -\frac{\lambda_{\min}(\alpha P - \eta I)}{\lambda_{\max}(P)} V_a + \frac{1}{2\eta} P_{L2} \tilde{\mathbf{h}}_a \end{aligned} \quad (75)$$

From theorem 1, the fixed time of the estimation error in the observer is bounded. In other words, there is a positive constant Δ_a , and $\|\mathbf{h}_a\|_2 \leq \Delta_a$. Then, Eq. (75) can be scaled as follows:

$$\dot{V}_a \leq -\frac{\lambda_{\min}(\alpha P - \eta I)}{\lambda_{\max}(P)} V_a + \frac{1}{2\eta} \|P_L\|_2 \Delta_a = -K_a V_a + C_a \quad (76)$$

where $K_a = \frac{\lambda_{\min}(\alpha P - \eta I)}{\lambda_{\max}(P)}$ and $C_a = \frac{1}{2\eta} \|P_L\|_2 \Delta_a$. By solving differential inequality (76), the following can be obtained:

$$V_a \leq V_a(0) e^{-K_a t} + \frac{C_a}{K_a} (1 - e^{-K_a t}) \quad (77)$$

where $V_a = \frac{C_a}{K_a}$ as $t \rightarrow \infty$. Therefore, the closed-loop system is ultimately uniformly bounded and converges to the following neighborhood.

$$\Theta_a = \left\{ \mathbf{x}_a^{(0\Box 1)} \mid \left(\mathbf{x}_a^{(0\Box 1)} \right)^T P(A_{01}) \mathbf{x}_a^{(0\Box 1)} \leq \frac{K_a}{C_a} \right\} \quad (78)$$

The proof is complete.

Acknowledgements

This work was supported by the National Natural Science Foundation of China (Grant No.52272358, No.62103052).

Conflict of interest statement

The authors declare that they have no conflicts of interest to this work.

References

- [1] Z. Shi, L. Zhao, Robust model reference adaptive control based on linear matrix inequality, *Aerospace Science and Technology*, 66 (2017) 152-159.
- [2] L. Zhao, Z. Shi, Y. Zhu, Acceleration autopilot for a guided spinning rocket via adaptive output feedback, *Aerospace Science and Technology*, 77 (2018) 573-584.
- [3] S. Talole, A. Godbole, J. Kolhe, S. Phadke, Robust roll autopilot design for tactical missiles, *Journal*

- of guidance, control, and dynamics, 34 (2011) 107-117.
- [4] Z. Shi, L. Zhao, Z. Liu, Variational method based robust adaptive control for a guided spinning rocket, *Chinese Journal of Aeronautics*, 34 (2021) 164-175.
 - [5] P. Trivedi, B. Bandyopadhyay, S. Mahata, S. Chaudhuri, Roll stabilization: a higher-order sliding-mode approach, *IEEE Transactions on Aerospace and Electronic Systems*, 51 (2015) 2489-2496.
 - [6] G. Duan, High-order fully actuated system approaches: Part IV. Adaptive control and high-order backstepping, *International Journal of Systems Science*, 52 (2021) 972-989.
 - [7] D. Guang-Ren, Direct parametric control of fully-actuated second-order nonlinear systems—The normal case, *Proceedings of the 33rd Chinese Control Conference, IEEE, 2014*, pp. 2406-2413.
 - [8] F. Xiao, L. Chen, Attitude control of spherical liquid-filled spacecraft based on high-order fully actuated system approaches, *Journal of Systems Science and Complexity*, 35 (2022) 471-480.
 - [9] X. Liu, M. Chen, L. Sheng, D. Zhou, Adaptive fault-tolerant control for nonlinear high-order fully-actuated systems, *Neurocomputing*, 495 (2022) 75-85.
 - [10] W. Liu, G. Duan, M. Hou, High - order robust command filtered backstepping design for strict - feedback systems: A high - order fully actuated system approach, *International Journal of Robust and Nonlinear Control*, 32 (2022) 10251-10270.
 - [11] L. Zhang, L. Zhu, C. Hua, Practical prescribed time control based on high-order fully actuated system approach for strong interconnected nonlinear systems, *Nonlinear Dynamics*, (2022) 1-11.
 - [12] S. Lu, K. Tsakalis, Y. Chen, Development and Application of a Novel High-Order Fully Actuated System Approach—Part I: 3-DOF Quadrotor Control, *IEEE Control Systems Letters*, 7 (2022) 1177-1182.
 - [13] Z. Li, Y. Zhang, R. Zhang, Prescribed error performance control for second-order fully actuated systems, *Journal of Systems Science and Complexity*, 35 (2022) 660-669.
 - [14] P. Tang, F. Zhang, J. Ye, D. Lin, An integral TSMC-based adaptive fault-tolerant control for quadrotor with external disturbances and parametric uncertainties, *Aerospace Science and Technology*, 109 (2021) 106415.
 - [15] H. Wang, L. Shi, Z. Man, J. Zheng, S. Li, M. Yu, C. Jiang, H. Kong, Z. Cao, Continuous fast nonsingular terminal sliding mode control of automotive electronic throttle systems using finite-time exact observer, *IEEE Transactions on Industrial Electronics*, 65 (2018) 7160-7172.
 - [16] Y.B. Shtessel, I.A. Shkolnikov, A. Levant, Smooth second-order sliding modes: Missile guidance application, *Automatica*, 43 (2007) 1470-1476.
 - [17] J. Xia, H. Ouyang, Chattering Free Sliding Mode Controller Design for Underactuated Tower Cranes With Uncertain Disturbance, *IEEE Transactions on Industrial Electronics*, (2023).
 - [18] P. Tang, D. Lin, D. Zheng, S. Fan, J. Ye, Observer based finite-time fault tolerant quadrotor attitude control with actuator faults, *Aerospace Science and Technology*, 104 (2020) 105968.
 - [19] Y. Ji, D. Lin, W. Wang, S. Hu, P. Pei, Three-dimensional terminal angle constrained robust guidance law with autopilot lag consideration, *Aerospace Science and Technology*, 86 (2019) 160-176.
 - [20] H. Rabiee, M. Ataei, M. Ekramian, Continuous nonsingular terminal sliding mode control based on adaptive sliding mode disturbance observer for uncertain nonlinear systems, *Automatica*, 109 (2019) 108515.
 - [21] W. Xu, S. Qu, L. Zhao, H. Zhang, An improved adaptive sliding mode observer for middle-and high-speed rotor tracking, *IEEE transactions on power electronics*, 36 (2020) 1043-1053.
 - [22] Y. Zhu, J. Qiao, L. Guo, Adaptive sliding mode disturbance observer-based composite control with prescribed performance of space manipulators for target capturing, *IEEE Transactions on Industrial Electronics*, 66 (2018) 1973-1983.
 - [23] A. Polyakov, Nonlinear feedback design for fixed-time stabilization of linear control systems, *IEEE Transactions on Automatic Control*, 57 (2011) 2106-2110.
 - [24] Z. Zuo, L. Tie, Distributed robust finite-time nonlinear consensus protocols for multi-agent systems, *International Journal of Systems Science*, 47 (2016) 1366-1375.
 - [25] L. Cao, B. Xiao, M. Golestani, D. Ran, Faster fixed-time control of flexible spacecraft attitude stabilization, *IEEE Transactions on Industrial Informatics*, 16 (2019) 1281-1290.
 - [26] Z. Zuo, Nonsingular fixed-time consensus tracking for second-order multi-agent networks, *Automatica*, 54 (2015) 305-309.
 - [27] J.P. Mishra, C. Li, M. Jalili, X. Yu, Robust second-order consensus using a fixed-time convergent sliding surface in multiagent systems, *IEEE Transactions on Cybernetics*, 50 (2018) 846-855.
 - [28] S. Yu, X. Long, Finite-time consensus for second-order multi-agent systems with disturbances by integral sliding mode, *Automatica*, 54 (2015) 158-165.

- [29] B. Jiang, Q. Hu, M.I. Friswell, Fixed-time attitude control for rigid spacecraft with actuator saturation and faults, *IEEE Transactions on Control Systems Technology*, 24 (2016) 1892-1898.
- [30] M.L. Corradini, A. Cristofaro, Nonsingular terminal sliding-mode control of nonlinear planar systems with global fixed-time stability guarantees, *Automatica*, 95 (2018) 561-565.
- [31] Q. Chen, X.-G. Yan, Z. Wang, J. Mu, Variable structure attitude control for a rolling aerial vehicle via extended state observer, 2016 14th International Workshop on Variable Structure Systems (VSS), IEEE, 2016, pp. 379-384.
- [32] K. Li, S. Yang, L. Zhao, Stability of spinning missiles with an acceleration autopilot, *Journal of Guidance, Control, and Dynamics*, 35 (2012) 774-786.
- [33] X. Yan, S. Yang, F. Xiong, Stability limits of spinning missiles with attitude autopilot, *Journal of guidance, control, and dynamics*, 34 (2011) 278-283.
- [34] H. Wang, L.H. Shi, Z.H. Man, J.C. Zheng, S.H. Li, M. Yu, C.H. Jiang, H.F. Kong, Z.W. Cao, Continuous Fast Nonsingular Terminal Sliding Mode Control of Automotive Electronic Throttle Systems Using Finite-Time Exact Observer, *IEEE Transactions on Industrial Electronics*, 65 (2018) 7160-7172.
- [35] H. Wang, Z.H. Man, W.X. Shen, Z.W. Cao, J.C. Zheng, J. Jin, D.M. Tuan, Robust Control for Steer-by-Wire Systems With Partially Known Dynamics, *IEEE Transactions on Industrial Informatics*, 10 (2014) 2003-2015.
- [36] G. Duan, High-order system approaches: I. Fully-actuated systems and parametric designs, *Acta Automatica Sinica*, 46 (2020) 1333-1345.
- [37] Y.S. ZHANG Kuanqiao, LI Baochen, LIU Chang, Fixed-time convergent guidance law considering autopilot dynamics, *ACTA AERONAUTICA ET ASTRONAUTICA SINICA*, 40 (2019) 259-273.
- [38] X. Wang, J. Wang, Partial integrated missile guidance and control with finite time convergence, *Journal of Guidance, Control, and Dynamics*, 36 (2013) 1399-1409.
- [39] X. Shao, H. Wang, Active disturbance rejection based trajectory linearization control for hypersonic reentry vehicle with bounded uncertainties, *ISA transactions*, 54 (2015) 27-38.
- [40] C. Qi, W. Xugang, Y. Jing, W. Zhongyuan, Acceleration tracking control for a spinning glide guided projectile with multiple disturbances, *Chinese Journal of Aeronautics*, 33 (2020) 3405-3422.

Declaration of interests

The authors declare that they have no known competing financial interests or personal relationships that could have appeared to influence the work reported in this paper.

The authors declare the following financial interests/personal relationships which may be considered as potential competing interests:

Journal Pre-proof